Optimal Single Stage Restoration of Split Beam Sonar Images via Mathematical Morphology

Larry R. Rystrom[1,2] Robert M. Haralick[2,1] Philip L. Katz[1,2]

[1]Applied Physics Laboratory,
[2]Department of Electrical Engineering
University of Washington, Seattle, WA 98195.

Abstract

Split beam sonar binary images are inherently noisy and have large quantities of "shot" noise as well as many missing data points. We address the problem of their restoration via Mathematical Morphology. Conventional restoration techniques for these types of images do not make use of any of the spatial relationships between data points, such as a qualitative observation that outliers tend to have a much larger distances to neighboring pixels. We first define an explicit noise model that characterizes the image degradation process for split beam sonar images. A key feature of the model is that the degradation is split into two parts, a foreground component and a background component. The amount of noise occuring in the background decreases with distance from the underlying signal object. Thus outliers in the model have the same statistical properties as those observed in training data. Next we propose two different restoration algorithms for this these kinds of images based respectively on morphological distance transforms and dilation with a toroid shaped structuring element followed by intersection. Finally we generalize to processing other kinds of imagery where applicable.

1 Introduction

Noise manages to corrupt most images that are of interest in digital image processing. It makes detecting and estimating desired quantities more difficult. With increased understanding of how noise corrupts images, it should be possible to design better and more robust mathematical morphological ([1]) algorithms that are less sensitive to noise. Split beam sonar images are an instance of a mixed noise corruption process that both removes foreground pixels and adds background noise to an image. Before further processing can proceed is is desirable to try and undo some of the effects of the noise. If the noise model is explicit, algorithm structure design may become easier, algorithm performance can be quantified, and algorithms can be designed for new classes of imagery without even viewing them.

Prior work in design of morphological algorithms has focussed mainly on algorithm performance in terms of training data, rather than with an explicit noise model ([2],[3]) whereby a sample mean is minimized rather than an expectation. Alternatively, one sided subtractive (additive) noise has been assumed in [4], [5], [6], [7], [8],and [9]. The "germ grain" mixed noise model described in [10] and [11] defines an image degradation process in which "germs" fall on an image according to a known (Poisson typically) distribution. Each germ is then dilated with a "primary grain" selected from a different distribution which describes the noise at that point. If the grain is on the foreground it become subtractive noise, if the grain is on the background then it becomes additive (union) noise. The approach of [12],[13] was to minimize an error bound which depended on the grains and the image jointly obeying certain limiting geometric assumptions.

The mixed noise models in the literature other than the germ grain model are typically designed to describe degradation of document images under various conditions. Kanungo, Haralick, and Philips in [14] focus on document image formation including optical and perspective effects. In it a degradation model is proposed that also varies with distance. However, the distance is not Euclidean distance, and a different form is assumed for the degradation. There is also no discussion as to when the model is appropriate, and if so, how to estimate the parameters. In [15], the morphological pattern spectrum is used to characterize salt and pepper noise affecting document images, however this is used only to predict success of their recognition algorithm, not as a description of the noise process. Reference [16] assumes that image noise is necessarily additive and white, then proceeds to estimate the standard deviation. In [17], both additive and multiplicative noise are allowed, however it is

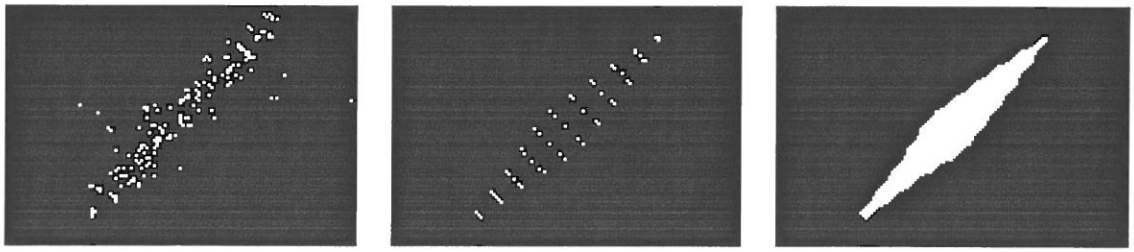

a b c

Figure 1: Illustrating split beam sonar image. a) Image b) Corresponding point scatterer model of underwater object c) Solid model formed from point scatterer model by closing with a large disk.

assumed that homogeneous regions of the image can first be successfully detected. For each homogeneous region, the kind of noise affecting it is then categorized.

In this paper we first describe some parts of the split beam image formation process. Secondly we describe a noise model which is more appropriate for our class of imagery than the noise models described in the literature. Next we propose two different restoration algorithms for these kinds of images based respectively on morphological distance transforms and dilation with a toroid shaped structuring element followed by intersection. The algorithms are judged by their performance in minimizing on the average, a point wise cost function. The algorithms are applicable to other kinds of imagery that follow the degradation model we describe.

2 Split Beam Sonar Imaging

Underwater acoustic imaging is a well developed field in its own right, references [18]-[20] are some of the many textbooks on the subject. The purpose of underwater acoustic imaging is to estimate quantities about underwater objects, such as location, orientation, shape, and speed, all by use of sound, rather than light. In this summary we concentrate on the split beam sonar model, the setup is that of Burdic ([18]). Split beam sonar, like all active sonars, broadcast a pulsed signal $s(t)$, then listens for the returned signal. Information about the underwater object must be inferred from the reflected signal after propagation through the water.

Before beginning a more detailed description of the fundamentals of split beam sonar, we first discuss qualitatively the reason for the large number of dropouts in a "typical" image (shown in Figure 1). The image was produced with the aid of the software package described in [22].

The large number of dropouts is explained by differences in dimensionality of the raw data versus the underlying three dimensional object. The raw data comes in 4-tuples of the form of (R, θ, ϕ, I), i.e. a location in spherical coordinates and an intensity *but the data is only taken along a single line* in three dimensional space. With noise effects, this means that a single discretized line is scattered among three dimensions. The relatively small number of data points of a single line in three dimensional space accounts for the sparseness phenomenon. An additional contributing factor is that when the intensity value is low then the data at that point is discarded as unreliable.

2.1 Split Beam Sonars

Split beam sonars provide a way to to estimate shape, location, and orientation of underwater objects. From the active sonar viewpoint, an underwater object is a collection of point scatterers, each acting like an individual point source when ensonified with pulse $s(t)$. In order to simplify the geometry we will describe the estimation procedure only for range and one angle, the extension to the other angle being similar. We will label the output of the three hydrophones (see Figure 2) $r_l(t)$, $r(t)$, and $r_r(t)$ corresponding to the left, middle, and right "beams."

For the particular split beam sonar model we are describing, sinusoidally modulated pulse $s(t)$ is assumed to be isotropic and emanate from center of the array (unlike light sensors, acoustic transducers can transmit as well as receive). After broadcasting, the received signals (after some preprocessing) are in the form of a "baseband complex" signal (see [23]), information about the sinusoidal carrier having been removed. In the split beam configuration the center channel will be used

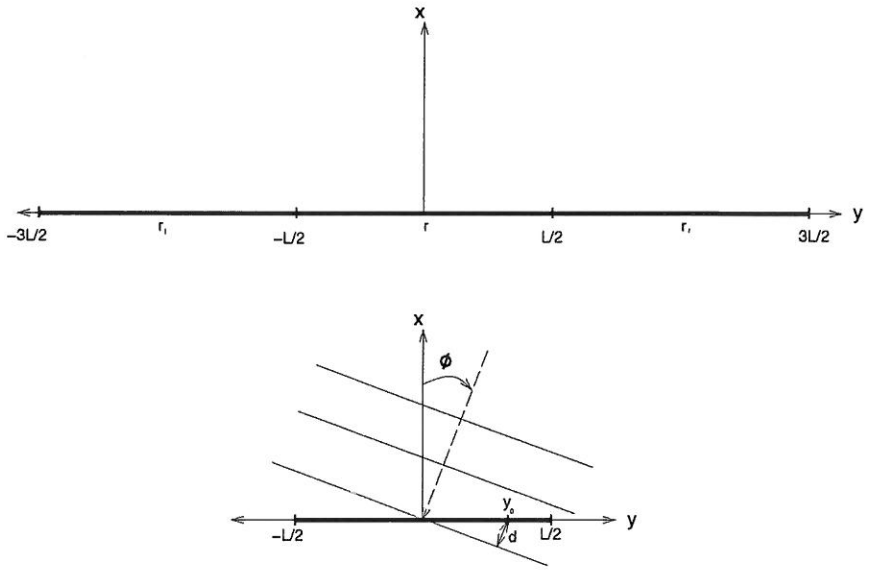

Figure 2: Illustrating split beam geometry. Top: The left hydrophone spans (-3L/2,-L/2), the middle hydrophone (-L/2,L/2), the right (L/2,3L/2). Bottom: A plane wave is incident on a single hydrophone. Consider a point along the y axis designated as the origin, and a displacement y_0 along that axis, then at the origin, the signal is delayed as compared to the signal received at y_0, by an amount $d = y_0 \sin(\phi)$.

to estimate range (intensity) while the left and right channels will be used to to estimate angle. The range and angle estimates are only declared "valid" when the amplitude is above a preset threshold ($I > T$).

2.2 Angle Estimation

For this derivation (taken largely from Burdic, [18]) we will make the simplifying far field assumption that the returned spherical wave is approximately a plane wave by the time it reaches the sensor. We also initially assume only one receiver. See Figure 2.

Let the signal at the origin be $R(t)$, then the received signal at any point on the y axis is given by $R(t, y, \phi) = R(t + \frac{y \sin(\phi)}{c})$. The output of the sensor (hydrophone) is given by

$$R_o(t, \phi) = \int_{\infty}^{-\infty} g(y) R(t + y \frac{\sin(\phi)}{c})\, dy$$

in general, where aperture function $g(y)$ describes the sensitivity of the hydrophone along the y axis. For the special case where $R(t)$ is a pure sinusoid we can write (using complex exponentials without any loss of generality) $R(t) = e^{j 2\pi f_0 t}$. For this case

$$\begin{aligned} R_o(t, \phi) &= \int_{\infty}^{-\infty} g(y) R(t + y \frac{\sin(\phi)}{c})\, dy \\ &= \int_{\infty}^{-\infty} g(y) e^{j 2\pi f_0 (t + y \frac{\sin(\phi)}{c})}\, dy \\ &= \left[\int_{-\infty}^{\infty} g(y) e^{j 2\pi \frac{\sin(\phi) f}{c} y}\, dy \right] e^{j 2\pi f_0 t} \\ &= G(f_0, \phi) e^{j 2\pi f_0 t} \end{aligned}$$

where

$$G(f, \phi) = \int_{-\infty}^{\infty} g(y) e^{j 2\pi \frac{\sin(\phi) f}{c} y}\, dy$$

corresponds to the Fourier transform of $g(y)$ with frequency variable $\frac{\sin(\phi)f}{c}$. The complex baseband version of the signal is given by

$$r(t,\phi) = [R_o(t,\phi)e^{-j2\pi f_0 t}]_{LP} = [G(f_0,\phi)]_{LP} = G(f_0,\phi)$$

The complex baseband signal is formed by multiplication with a complex number corresponding to broadcast frequency, then low pass filtering the result. Note that low pass filtering a constant (or zero frequency component) leaves it unchanged.

At this point we "split" the hydrophone into two channels and adopt the geometry at the top of Figure 2. $g(y)$ is effectively split into a left channel $g_l(y) = g(y+L)$ and a right channel $g_r(y) = g(y-L)$. The corresponding Fourier transforms are

$$G_l(f,\phi) = G(f,\phi)e^{j2\pi\frac{\sin(\phi)f}{c}L}$$

$$G_r(f,\phi) = G(f,\phi)e^{-j2\pi\frac{\sin(\phi)f}{c}L}$$

since the effect of translation in one domain is frequency scaling in the other. The complete signal at each hydrophone is then

$$r_l(t,\phi) = G(f_0,\phi)e^{j2\pi\frac{\sin(\phi)f_0}{c}L}$$

$$r_r(t,\phi) = G(f_0,\phi)e^{-j2\pi\frac{\sin(\phi)f_0}{c}L}$$

A new signal can be formed by combining the left and right channels as

$$\begin{aligned} r_l(t,\phi)r_r^*(t,\phi) &= |G(f_0,\phi)|^2 e^{j4\pi\frac{\sin(\phi)f_0}{c}L} \\ &= |G(f_0,\phi)|^2\left[\cos(4\pi\frac{\sin(\phi)f_0}{c}L) + jk\sin(4\pi\frac{\sin(\phi)f_0}{c}L)\right] \end{aligned}$$

Upon taking the ratio of the real and imaginary parts of $r_l(t,\phi)r_r^*(t,\phi)$ we have

$$\frac{Im\{r_l r_r^*\}}{Real\{r_l r_r^*\}} = \tan(4\pi L\frac{\sin(\phi)f_0}{c})$$

provided that $|G(f_0,\phi)|^2 \neq 0$ (it is not a null location in the window function).
Finally,

$$\phi = \sin^{-1}(\frac{\tan^{-1}(\frac{Im\{r_l r_r^*\}}{Real\{r_l r_r^*\}})}{4\pi L f_0/c})$$

Performance of this estimator under noisy conditions is discussed in [18] and [24].

2.3 Image Formation

The image shown in Figure 1.a was formed in the following way. First the split beam sonar processing model was applied to the output of a run of the SST simulator (reference [22]). The R and ϕ components of the original data vector were then used to form X and Y components which was then discretized into row and column positions on the image. The reason that ϕ rather than θ was used can be understood in terms of the variances of the angle estimates, in particular $Var\{\hat{\phi}\} \leq Var\{\hat{\theta}\}$. The angles estimates are better in the left/right direction than the top/bottom direction because of interference and reverberation from the sea surface and sea bottom. Another contributing factor is change in the speed of sound with depth.

An alternative approach to image formation (not followed) would be to convert from spherical coordinates to rectangular coordinates. This would produce a list of 3-tuples of the form (X, Y, Z). An orthographic projection coule then be performed by dropping the Z coordinate. However this neglects the effects of the vertical angle component.

3 A Mixed Noise Model for Split Beam Sonar Imagery

The model, which describes the degradation process from an ideal image A to a random image $\underline{C}$ can be succinctly stated in terms of two equations:

$$p(x = 1|x \in R_r) = \alpha e^{-\delta r} \quad (1)$$

$$p(x_1 \in R_r, x_2 \in R_r, \ldots, x_{\#R_r} \in R_r) = \prod_{i=1}^{\#R_r} p(x_i \in R_r) \quad (2)$$

where

$$R_r = R_r(A) = \{x | r - 1 < d(x, A) \leq r\}$$

with

$$d(x, A) = \min_{a \in A} d(x, a)$$

defines a set of points that form a ring around object A. Equation 1 states that the probability of pixel located at x turning on is proportional to the negative exponential of its distance r to its closest point in A while equation 2 states that probabilities of pixels within the same ring turning on are independent from each other. R_r is easily computed in practice through the use of morphological distance transforms. In particular we shall use the "CHAMFER-5-7-11" distance transform structuring element described in [27]. With this approach, the computed distance is always within 2% of the Euclidean. For more details concerning model validation and estimation of model parameters see [21].

4 Maximum A Posteriori Estimation

A key feature of the noise model is being able to calculate $p(\underline{C} = C|A)$ which is the probability of a particular random image occuring, given the noise model (dependence on the noise model parameters is suppressed here, if not known they may have to be estimated from training data). On the other given a particular C, we would like to estimate which A it came from. Following Bayes rule we write,

$$p(A|C) = \frac{p(C|A)\pi(A)}{p(C)}$$

where $p(C) = \sum_A p(C|A)\pi(A)$. The posterior distribution of A completely describes our state of knowledge of A. If A were a continuous random variable, then a reasonable estimate of A could be obtained by the expected value. However, since A is a discrete random set, we prefer to estimate it by the mode of the distribution, i.e. select that value of A which maximizes $p(A|C)$. This is known as maximum a posteriori (MAP) estimation. For the specific case of the noise model of the last chapter (with parameters α, δ, and L) and assuming that A is random in the sense in the sense of unknown location and assuming uniform priors (in practical situations it may be known with higher probability where A is on the image),

$$\begin{aligned}
\hat{A} &= \operatorname*{argmax}_A p(A|C) \\
&= \operatorname*{argmax}_A \frac{p(C|A)\pi(A)}{p(C)} \\
&= \operatorname*{argmax}_A p(C|A) \\
&= \operatorname*{argmax}_{A_t} p(C|A_t) \\
&= \operatorname*{argmax}_t \prod_{r=0}^{r_{max}} (\alpha e^{-r\delta})^{\#(R_r \cap C)} \times (1 - \alpha e^{-r\delta})^{\#R_r - \#(R_r \cap C)}
\end{aligned}$$

where R_r is the r^{th} ring around A_t.

The optimum estimation procedure in this scheme is found by a sort of template matching. The shape A is moved around on the image and the probability of its occuring is calculated according to the noise model.

5 Generalized Set Symmetric Difference Based Estimation

At this point we switch to making our estimation based on an entirely different set of principles. We suppose that we are trying to minimize

$$E\{d(\underline{\mathrm{A}}, \Psi(\underline{\mathrm{C}}))\}$$

where algorithm Ψ is under our control. In the most general setting d is primarily a cost function rather than being a distance measure. The value of $d(A, \hat{A})$ determines the cost we will assign to estimating A as $\hat{A}$. We propose the following form:

$$d(A, C) \equiv \sum_{c \in C - A} d(c, A) + \sum_{a \in A - C} d(a, A^c)$$

where

$$d(a, B) \equiv \min_{b \in B} d(a, b)$$

returns the distance from a point to a set.

The first term of the cost function penalizes excessive pixels by their distance from the true underlying object. The second term of the cost function penalizes missing pixels by their distance from the object boundary. In effect, pixels near the center of the object are considered more valuable in terms of restoration than those right near the edge. The proposed cost function is a compromise between the set symmetric distance metric

$$d_{sd}(A, C) = \#(C - A) + \#(A - C)$$

which operates point wise and takes no account of shape and the Hausdorf metric ([5],[6],[1]) metric which takes into account the shape of two sets when assigning a distance between two sets. Since the second term of the cost function is not symmetric to the first it is apparent that the cost function is not at metric except in the special case that $d(a, c) = 1 - \delta[a, c]$ which reduces the cost function to the symmetric set difference distance. Before proceeding, we note that the generalized set symmetric difference measure can be expressed in term of the symmetric set difference as follows:

$$d(A, C) = \sum_{i=1}^{\infty} d_{sd}(C \cup (A \oplus disk(i)), A \oplus disk(i)) + \sum_{i=1}^{\infty} d_{sd}(C \cap (A \ominus disk(i)), A \ominus disk(i))$$

In terms of minimizing the expected distance if

1. $\underline{\mathrm{A}} = A_{\underline{\mathrm{t}}}$ ($\underline{\mathrm{A}}$ is random only in the sense of unknown location)
2. $p(C|A) = p(C_t|A_t)$ (the noise model is translation invariant)
3. $\Psi(C_t) = \Psi(C)_t$ (the restoration algorithm is translation invariant)

all hold then,

$$E\{d(\underline{\mathrm{A}}, \Psi(\underline{\mathrm{C}}))\} = E\{d(A, \Psi(\underline{\mathrm{C}}))\}$$

which says that during minimization knowledge of A is allowed.

Distributing expectation over sums produces:

$$\begin{aligned} E\{d(A, \Psi(\underline{\mathrm{C}}))\} &= E\{ \sum_{c \in \Psi(\underline{\mathrm{C}}) - A} d(c, A) + \sum_{a \in A - \Psi(\underline{\mathrm{C}})} d(a, A^c)\} \\ &= \sum_{c \in Total(A, \Psi) - A} p(c \in \Psi(\underline{\mathrm{C}})) d(c, A) + \sum_{a \in A} p(c \notin \Psi(\underline{\mathrm{C}})) d(a, A^c) \end{aligned}$$

The pointwise probabilities that the noise model must provide are the probability a pixel is on (off) after filtering with Ψ and knowledge about the spatial extent of the noise with respect to A, denoted by $Total(A, \Psi)$ after filtering with Ψ.

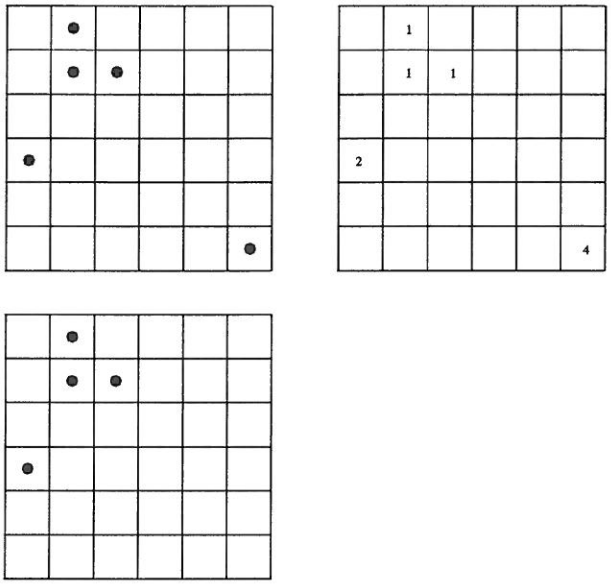

Figure 3: Illustrating filtering based on nearest neighbor distance. In the example pixels with a chessboard distance of more than three are removed.

6 Nearest Neighbor Distance Algorithm

Given the noise model of the previous chapter, we might intuitively expect that points in the outer rings, are a long distance away from nearest neighbors. One filtering approach would be to remove points in $\underline{C}$ that are more than a certain distance from their nearest neighbor, specifically,

$$\Psi(C;k) = C \cap (NN(C) \leq k)$$

where $NN(C)$ returns an image with each foreground pixel labeled with its nearest neighbor distance. Note that small values of k correspond to more severe filtering. See Figure 3 for an illustration of nearest neighbor based filtering.

With Ψ in the above form, a pixel is in C after filtering if it was in C before filtering, and if it had a neighbor within a distance of k. Therefore,

$$p(c \in \Psi(\underline{C};k)) = p(c \in \underline{C} \text{ and } (disk_{-0}(k))_c \cap \underline{C} \neq \phi)$$

Here $disk_{-0}(k) = disk(k) - \{0\}$ is the disk of the corresponding size with the origin removed. The equation simplifies to

$$p(c \in \Psi(\underline{C};k)) = p(c \in \underline{C})(1 - \prod_{d \in (disk_{-0})_c} (1 - p(d \in \underline{C})))$$

where $p(c \in \underline{C}) = \alpha e^{-d(c,A)\delta}$ is calculated in terms of the noise model parameters α and δ.

Figure 4 shows the performance curves of this sort of filter. We note the rather good agreement between the threshold value predicted from the model, and that obtained from the data. As the cost function has two terms that correspond to under and over filling and sum to the overall error, so too these performance curves are presented in Figure 5.

6.1 Computation of Nearest Neighbor Distance

The distance from each pixel to its nearest neighbor is computed as a variant of recursive morphological distance transform algorithm. During each of the four passes, each pixel broadcasts its distance in one of four quadrants. The passes are made in the top-bottom-left-right, top-bottom-right-left, bottom-top-right-left, and bottom-top-left-right, order which respectively

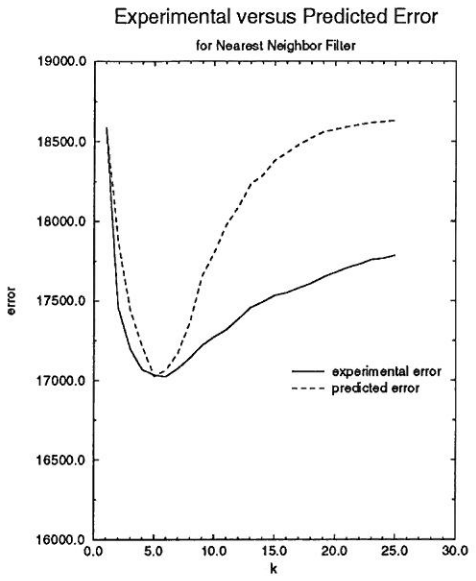

Figure 4: Illustrating theoretical versus experimental performance of the nearest neighbor filtering algorithm on the split beam sonar image data set. Small values of k correspond to more severe filtering.

broadcast in the fourth, third, second, and first quadrants. In turn, each foreground pixel also records the smallest distance it received during each of the four broadcasts.

Let K be the structuring element that determines choice of distance and let K_1, K_2, K_3, and K_4 represent subsets of K used during each pass, defined as follows:

$$\begin{aligned} K_1 &= \{k \in K | k.row \leq 0, k.col \leq 0, k \neq 0\} \\ K_2 &= \{k \in K | k.row \leq 0, k.col \geq 0, k \neq 0\} \\ K_3 &= \{k \in K | k.row \geq 0, k.col \leq 0, k \neq 0\} \\ K_4 &= \{k \in K | k.row \geq 0, k.col \geq 0, k \neq 0\} \end{aligned}$$

Let the dimension of input image I be $\{0, \ldots, M-1\} \times \{0, \ldots, N-1\}$ and let J be a temporary work image with domain $I \oplus K$ and

$$J(r,c) = \begin{cases} d_{max} & \text{if}(r,c) \in \{(-1,0),(-1,N-1),(M,0),(M,N-1)\} \\ 0 & \text{otherwise} \end{cases}$$

initially where d_{max} is the length of the image diagonal. Setting a pixel near each corner to this value ensures that if image I consists of only two foreground pixels in each corner, it will still be correctly labelled. At the end of the four passes, each foreground pixel in I will be labelled with the distance to its nearest neighbor; this result will be in image D.

1. For each pixel $(r,c) \in I$ in top-bottom-left-right order:

   $e = \min_{k \in K_1} \{J(r,c) + K_1(r,c)\}$
   if $I(r,c) = 0$ then $J(r,c) = e$
   else
   $J(r,c) = 0$
   $D(r,c) = e$

2. For each pixel $(r,c) \in I$ in top-bottom-right-left order:

   $e = \min_{k \in K_2} \{J(r,c) + K_2(r,c)\}$

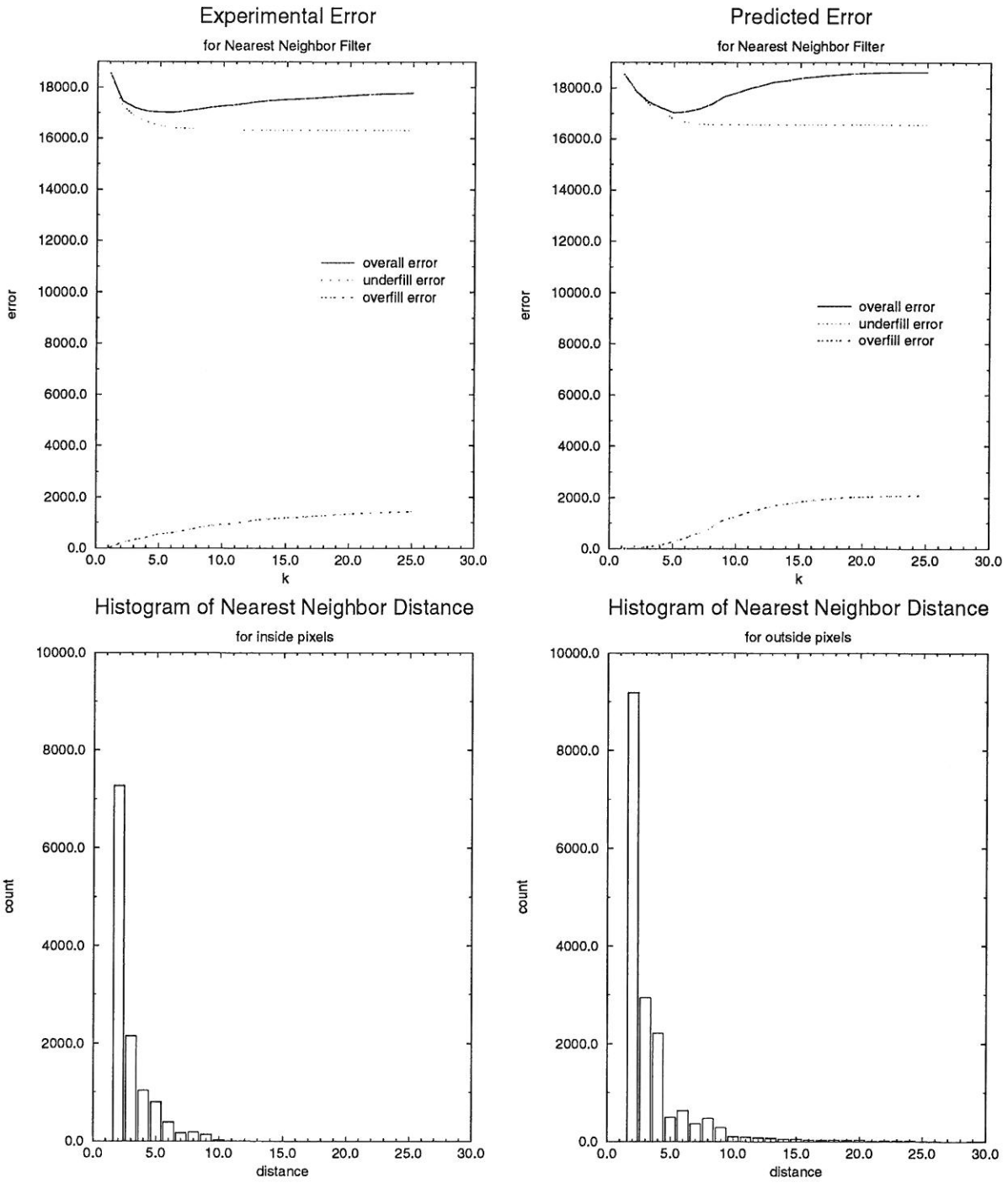

Figure 5: Illustrating theoretical versus experimental performance of the nearest neighbor filtering algorithm on the split beam sonar image data set. The overall error is the sum of an underfill error term and an overfill error term. This is shown in the top row. The bottom row shows nearest neighbor distance histograms for both the "inside" part of C ($C \cap A$) and the "outside" part of C ($C - A$). The effect of thresholding at nearest neighbor distance k is to remove all nearest neighbor values to the right of k in the histograms.

if $I(r,c) = 0$ then $J(r,c) = e$
else
$J(r,c) = 0$
$D(r,c) = \min\{D(r,c), e\}$

3. For each pixel $(r,c) \in I$ in bottom-top-right-left order:

$e = \min_{k \in K_3} \{J(r,c) + K_3(r,c)\}$
if $I(r,c) = 0$ then $J(r,c) = e$
else
$J(r,c) = 0$
$D(r,c) = \min\{D(r,c), e\}$

4. For each pixel $(r,c) \in I$ in bottom-top-left-right order:

$e = \min_{k \in K_4} \{J(r,c) + K_4(r,c)\}$
if $I(r,c) = 0$ then $J(r,c) = e$
else
$J(r,c) = 0$
$D(r,c) = \min\{D(r,c), e\}$

7 Dilation with Toroid Shaped Structuring Element Algorithm

The previous algorithm generalizes to dilation with a toroid or ring shaped structuring element.

$$\Psi(C; k_1, k_2) = C \cap (C \oplus toroid(k_1, k_2))$$

With Ψ in the above form, a pixel is in C after filtering if it was in C before filtering, and if it had a neighbor within the toroid shape centered at that point. Therefore,

$$p(c \in \Psi(\underline{C}; k_1, k_2)) = p(c \in \underline{C} \text{ and } (disk(k1) - disk(k2))_c \cap \underline{C} \neq \phi)$$

The equation simplifies to

$$p(c \in \Psi(\underline{C}; k)) = p(c \in \underline{C})(1 - \prod_{d \in (disk(k_1) - disk(k_2))_c} (1 - p(d \in \underline{C})))$$

where $p(c \in \underline{C}) = \alpha e^{-d(c,A)\delta}$ is calculated in terms of the noise model parameters α and δ.

8 Conclusions

We defined an image degradation model which described how noise corrupts split beam sonar binary images and turns them into the kinds of images actually observed. After describing the model we proposed two different algorithms for image restoration of these kinds of images. The experimental results were in close agreement to those predicted by the model.

9 Acknowledgements

Mr. Rystrom gratefully acknowledges the support he received from the Applied Physics Laboratory of the University of Washington.

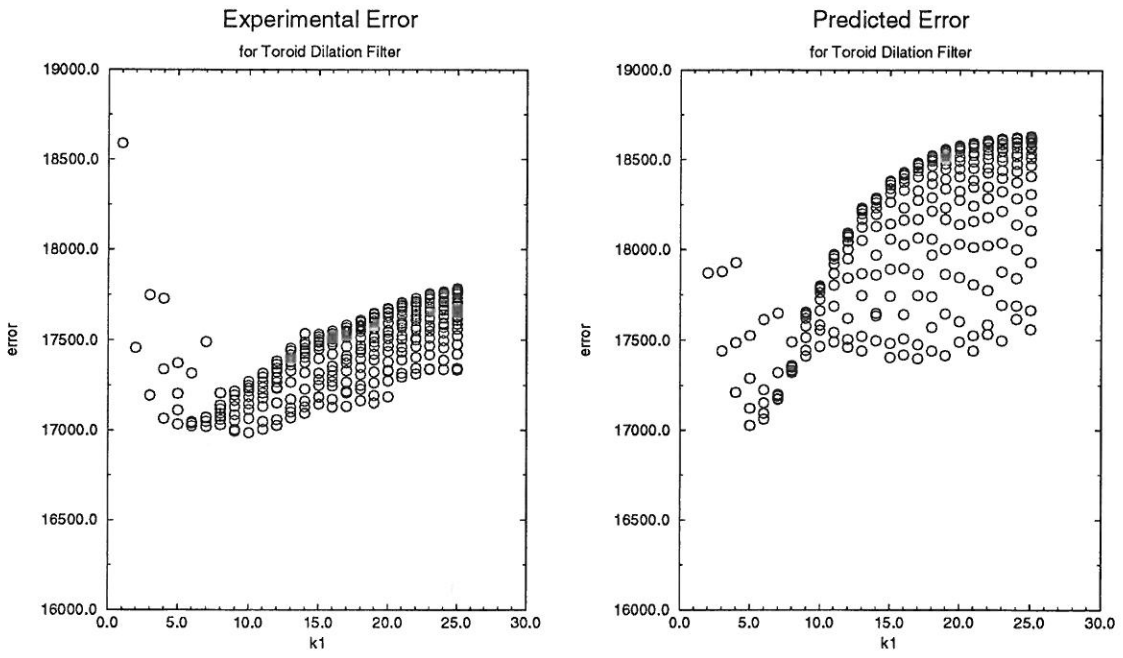

Figure 6: Illustrating theoretical versus experimental performance of the dilation followed by intersection algorithm on the split beam sonar image data set. The x axis corresponds to the outer diameter parameter k_1 of the toroid shape structuring element. The error values for toroids with corresponding inner diameter $k_2, 1 \ldots k_1 - 1$ are plotted for each k_1.

References

[1] R. M. Haralick and L. G. Shapiro, *Computer and Robot Vision*, Vol. 1, Addison-Wesley, Reading, Massachusetts, 1992.

[2] L.R. Rystrom, P. L. Katz, R.M. Haralick, C.J. Eggen, "Morphological Algorithm Development Case Study: Detection of Shapes in Low Contrast Gray Scale Images with Replacement and Clutter Noise", *SPIE Proceedings, Nonlinear Image Processing III*, Vol. 1658, February 12-13 1992, pp. 76-93.

[3] Robert P. Loce, Edward R. Dougherty, "The Morphological Filter Mean-Absolute Error Theorem", Proceedings of the SPIE, Vol. 1658, February 1992.

[4] Larry R. Rystrom, Robert M. Haralick, Philip L. Katz, "Optimal Dilation Filtering", *Proceedings of the Canadian Conference on Electrical and Computer Engineering*, Toronto, Ontario, September 1992, pp.TA3.19.1 - TA3.19.4.

[5] Larry R. Rystrom, Robert M. Haralick, Philip L. Katz, "Optimal Single Stage Restoration of Subtractive Noise", Proceedings of the SPIE, Vol. 1902, pp. 8-19, February 1993.

[6] Larry R. Rystrom, Robert M. Haralick, Philip L. Katz, "Optimal Single Stage Restoration of Subtractive Noise by a Morphological Closing", Submitted to the SPIE Journal of Electronic Imaging.

[7] Ian Joughin, Robert M. Haralick, Edward R. Dougherty, "A Model Based Algorithm for Designing Suboptimal Morphological Filters for Restoring Subtractive-Noise-Corrupted Images", submitted to the SPIE Journal of Electronic Imaging.

[8] Edward R. Dougherty, "Optimal Mean Square N-Observation Digital Morphological Filters Part I: Optimal Binary Filters", *Journal of Computer Vision, Graphics, and Image Processing: Image Understanding*, Vol. 55, no 1.,January 1992.

[9] Edward R. Dougherty, "Optimal Mean Square N-Observation Digital Morphological Filters Part II: Optimal Gray Scale Filters", *Journal of Computer Vision, Graphics, and Image Processing: Image Understanding*, Vol. 55, no 1.,January 1992.

[10] J. Serra, *Image Analysis and Mathematical Morphology*, Academic Press, Orlando, Florida, 1982.

[11] Noel Cressie, *Statistics for Spatial Data*, Wiley, New York, 1991.

[12] D. Schonfeld, J. I. Goutsias, "Optimal Morphological Filters for Pattern Restoration", *SPIE Vol. 1199, Visual Communication and Image Processing IV*, 1989.

[13] D. Schonfeld, J. I. Goutsias, "Optimal Morphological Pattern Restoration from Noisy Binary Images", *IEEE Trans. on Pattern Analysis and Machine Intelligence*, vol. 13, pp. 14-29, January 1991.

[14] Tapas Kanungo, Robert M. Haralick, Ihsin Phillips, "Global and Local Document Degradation Models", Proceedings of the International Conference on Document Analysis and Recognition, October 20-22, 1993, Tsukuba, Japan, 1993.

[15] V.P. Concepcion, M.P. Grzech, "Using Morphology and Associative Memories to Associate Salt-and-Pepper Noise with OCR error rates in document images", Proceedings of the SPIE, vol. 1661, pp.18-26, Feb. 1992.

[16] S.I. Olsen, "Estimation of Noise in Images: An Evaluation", CVGIP: Graphical Models and Image Processing, vol. 55, no. 4, pp. 319-23, July 1993.

[17] K. Chehdi, M. Sabri, "A New Approach to Identify the Nature of the Noise Affecting and Image", ICASSP-92, San Franciso, CA, March 1992.

[18] William S. Burdic, *Underwater Acoustic System Analysis*, Prentice-Hall, Englewood Cliffs, NJ, 1984.

[19] Robert J. Urick, *Principles of Underwater Sound for Engineers*, McGraw-Hill, New York, 1967.

[20] Richard O. Nielsen, *Sonar Signal Processing*, Artech House, Boston, 1991.

[21] Larry R. Rystrom, "Optimal Morphological Estimation and Filtering", Ph.D. thesis, University of Washington.

[22] Robert P. Goddard, "The Sonar Simulation Toolset", *Proceedings of Oceans 89*, (sponsor: Oceanic Engineering Society of the IEEE), Vol. 4, p. 1217, Seattle, WA September 1989.

[23] W.C. Knight, R.G. Pridham and S.M. Kay, "Digital Signal Processing for Sonar", *Proceedings of the IEEE*, 69 (11), p. 1451-1506, 1981.

[24] Didier Billon, "Bearing Estimation of a Single Monochromatic Plane Wave with a Linear Receiving Array", p. 773, *Progress in Underwater Acoustics*, Editor: Harold M. Merklinger, Plenum Press, New York, 1986.

[25] G. Clifford Carter, "Coherence and Time Delay Estimation", *Proceedings of the IEEE*, Vol. 75, No. 2, February 1987.

[26] Merrill I. Skolnik, *Introduction to Radar Systems*, McGraw-Hill, New York, 1980.

[27] Gunilla Borgefors, "Distance Transformations in Digital Images", Computer Vision, Graphics, and Image Processing 34, 344-371, (1986).